**Article:**
Yin, L. orcid.org/0000-0001-7148-0943, Cai, J., Ma, L. et al. (5 more authors) (2024) Dual function of magnetic nanocomposites-based SERS lateral flow strip for simultaneous detection of aflatoxin B1 and zearalenone. Food Chemistry, 446. 138817. ISSN 0308-8146

https://doi.org/10.1016/j.foodchem.2024.138817

# Dual function of magnetic nanocomposites-based SERS lateral flow strip for simultaneous detection of aflatoxin B1 and zearalenone

Limei Yin[a,b]*, Jianrong Cai[b], Lixin Ma[b], Tianyan You[a], Muhammad Arslan[b], Heera Jayan[b], Xiaobo Zou[b], Yunyun Gong[c]*

[a] *International Joint Research Laboratory of Intelligent Agriculture and Agri-products Processing, School of Agricultural Engineering, Jiangsu University, Zhenjiang 212013, China*

[b] *China Light Industry Key Laboratory of Food Intelligent Detection & Processing, School of Food and Biological Engineering, Jiangsu University, Zhenjiang 212013, China*

[c] *School of Food Science and Nutrition, University of Leeds, Leeds LS2 9JT, UK*

*Corresponding author at: School of Food and Biological Engineering, Jiangsu University, Zhenjiang 212013, China

Email address: yinlm6@163.com (L.M. Yin), Y.Gong@leeds.ac.uk (Y. Gong)

**Abstract:** Aflatoxin B1 (AFB1) and zearalenone (ZEN) are two mycotoxins that often co-occur in corn. A surface-enhanced Raman scattering-based lateral flow immunoassay (SERS-LFIA) that can simultaneously detect AFB1 and ZEN in corn samples was developed employing the core-interlayer-satellite magnetic nanocomposites ($Fe_3O_4$@PEI/$Au^{MBA}$@$Ag^{MBA}$) as dual-functional SERS tags. Under the optimal conditions, the detection ranges of AFB1 and ZEN in corn samples were 0.1-10 μg/kg and 4-400 μg/kg, respectively. Moreover, the test results for two mycotoxins in contaminated corn samples employing the suggested SERS-LFIA was in line with those of the HPLC technique. In view of its satisfactory sensitivity, accuracy, precision and short testing time (20 min), the developed system has a promising application prospect in the on-site simultaneous detection of AFB1 and ZEN.

***Keywords:*** Lateral flow; Aflatoxin B1; Zearalenone; Magnetic; $Fe_3O_4$; Surface-enhanced Raman scattering

# 1. Introduction

Corn, an indispensable commodity farmed worldwide since is employed as a raw material for both food and feed. The corn is considered one of the most susceptible grains to mildew during storage than other ones, owing to its large endosperm, amusing nutrients, vigorous respiration and a wide spectrum of infectious microbes (Kebede, et al., 2020). Mycotoxins are a hazardous category of secondary metabolites secreted by fungi of *Aspergillus, Fusarium* and *Penicillium* spp (Xie, et al., 2022). To date, approximately 400 mycotoxins have been discovered, among which zearalenone (ZEN), deoxynivalenol (DON), aflatoxin B1 (AFB1), ochratoxin A (OTA), fumonisins (FBs) as well as T-2 toxin (T2) which are furthermost commonly reported in the grain-food supply chain(Ji, Fan, & Zhao, 2016). Predominantly, co-contamination of multiple mycotoxins in corn is a pervasive manifestation, for instance combination of AFB1 and ZEN is thought to have one of the worst detrimental influences on living organisms` health (Xu, et al., 2016; Zhou & Tang, 2020). In this context, AFB1 is classified as a category 1A carcinogen due to its high toxicity and propensity for cancer (Ko, Lee, & Choo, 2015), whereas ZEN has a potent estrogen-like effect, which can obliterate the normal reproductive development in humans and animals (Yin, et al., 2023). Various motherlands and officialdoms have emanated the maximum residue levels (MRL) of AFB1 (2 ~ 20 μg/kg) and ZEN (20 ~ 300 μg/kg) in corn（Table S1) (W. Zhang, et al., 2020). However, once corn is consumed for special dietary meals such as baby, elder and patient food, substantially reduced MRL must be followed (Rebellato, et al., 2021). Basically, conventional approaches include high performance liquid

chromatography (HPLC), enzyme-linked immunosorbent assays (ELISA) in addition to liquid chromatography-mass spectrometry (LC-MS) are utilized for exposing mycotoxins (Xing, et al., 2020). Unfortunately, these procedures are quite complex, time-consuming and necessitate specialized equipment, making them inappropriate for rapid and on-site testing (Yang, et al., 2022). Furthermore, these techniques typically ascertain only one mycotoxin in a single run. Thus, it is imperative to develop a fast, convenient as well as accurate mode for the instantaneous detection of AFB1 and ZEN in corn.

Actually, immunochromatography is a simple and rapid diagnostic method, and a significant tool for point-of-care testing (POCT) (Wang, et al., 2021). Strips of lateral flow test based on gold nanoparticles (AuNPs) are the supreme archetypal immunochromatography contrivance, subscription swift analysis, economic, convenience, portability and visual analysis and have been extensively used in clinical diagnosis and food safety (Chen, et al., 2020; Lee, et al., 2019). Moreover, lateral flow immunoassay (LFIA) facilitates multi-channel analysis by scenery several Test (T) lines on the same nitrocellulose (NC) membrane (Wang, et al., 2017). Nevertheless, little sensibility and inadequate quantifiable capability of LFIA-based AuNPs obstruct their application in the recognition of trace analytes (Xing, et al., 2020). No doubt, introduction of innovative signal nanotags, including fluorescent microspheres, SERS-, and quantum dots, has piqued the interest of researchers to boost the sensitivity and quantitative capabilities of LFIA (Guo, et al., 2021; Kim, et al., 2021; Liu, et al., 2020). Among them, SERS tagging detection based on SERS nanotags

which lately has an ongoing outstanding reputation across a range of research applications owing to its extraordinary sensitivity, fast detection, anti-photobleaching and anti-quenching properties (Wang, et al., 2021). Typically, a representative SERS nanotag is constituted of 3 parts (Chen, et al., 2020): (i) gold or silver material-based core as the SERS substrates, (ii) Raman reporter molecules to construct robust distinctive Raman peaks, and (iii) recognition elements such as antibodies or aptamers to combine with the target analytes, which can assurance the sensibility, quantitative capability and specificity of SERS tagging examination assay. The Raman signal enhancement directly be contingent on the employed SERS substrates. Therefore, the design and manufacture of exceedingly active and multifunctional SERS substrates is crucial in refining the susceptibility and stability of SERS signals.

Electromagnetic (EM) enhancement is a major factor in magnifying the Raman signal, according to the SERS augmentation mechanism (Guo, et al., 2024; Pazos, et al., 2016). Commonly, EM enhancement engendered by localized surface plasmon resonance (LSPR) closes to the metal nanostructures surfaces or adjacent nanogaps which leads to generating enhancement sites with a very narrow scope, called "hotspots" (Liu, et al., 2022). Previously, several articles have reported that Au@Ag core-shell nanoparticles exhibited more excellent SERS performance than single type of nanoparticles (AuNPs and AgNPs) (Liu, et al., 2017). This is attributed to the fact that more hotspots can be generated at the core-shell intersection, which heightens the intensity and stability of the Raman peaks (Wang, et al., 2021). Today, SERS nanotags based on the core-shell of Au@AgNPs have been efficaciously utilized *via* variant

SERS-LFIA systems to achieve the sensitive detection of bacteria, veterinary drugs, pesticides, mycotoxins, etc (Ma, et al., 2023; Su, et al., 2021; Yin, et al., 2022; D. Zhang, et al., 2019; Zhang, et al., 2020). Nevertheless, the complex matrix interference in actual samples impacts the homogeneous distribution of hotspots in SERS immunocomplex on the test (T) lines, leading to random boost of Raman signals and rendering it unattractive for reproducible and quantitative SERS analysis. Auspiciously, magnetic SERS nanotags based on $Fe_3O_4$ were introduced to diminish matrix interference in the assembly of biosensors due to their excellent constancy and enrichment proficiency. Prior studies demonstrated that magnetic SERS nanotags ($Fe_3O_4$@Au and $Fe_3O_4$@Ag)-based SERS-LFIA was fruitfully equipped to the qualitative and quantitative inquiry of countless objectives, among them cancer biomarkers, viruses, and serum proteins (Liu, et al., 2020; Ren, et al., 2019; Wang, et al., 2019). Yet, magnetic SERS nanotags are prerequisites to be innovated for signal amplification ability, good dispersion, uniformity, stability and reproducibility. Since Au@Ag has greater enhancement and stability beside to iron NPs displays soft ferromagnetism, the amalgamation of $Fe_3O_4$ and Au@Ag may be a promising strategy to improve the performance of Au@Ag, subsequently showing a potent efficacy in wide spectrum of applications. Furthermore, recent findings revealed that the prepared multilayered magnetic-core dual-shell nanoparticle (MDAu@Ag) has superior SERS activity (Tu, et al., 2023). However, the preparation of MDAu@Ag requires four ultrasonic treatments to complete the adsorption of double layers of Au@Ag, making the synthesis process complex.

Through the present research, we constructed a bi-channel with ultrasensitive SERS-LFIA platform for the detection of two common mycotoxins (AFB1 and ZEN), that employed core-interlayer-satellite magnetic nanocomposites ($Fe_3O_4$@PEI/$Au^{MBA}$@Ag-MBA) as SERS tags. The progressions of our SERS-LFIA system can be abridged in three aspects. Firstly, high-performance $Fe_3O_4$@PEI/$Au^{MBA}$@Ag-MBA were familiarized into the LFIA system for the first time, serving as a promising dual functional tool for Raman signal amplification and immunocomplex enrichment. Polyethyleneimine (PEI) was used to adhere $Au^{MBA}$@Ag nanoparticles as satellites onto the $Fe_3O_4$ surface. Vitally, these fashioned magnetic SERS nanocomposites attain noble chemical stability, superior SERS activity, magnetism, monodispersity, and uncomplicatedness of preparation, thus ensuring potent sensitivity and repeatability. Secondly, the strong Raman signal and magnetic enrichment of SERS probes significantly improved the sensitivity of detection. This double amplification was attributed to the strong Raman signals provided by the double-layer of 4-MBA and the resuspension of magnetically enriched immunocomplex in running buffer at an enlarged concentration, occasioning a very strong Raman signal. Thirdly, testing duration were impressively reduced. The recommended SERS-LFIA strips accomplished simultaneous and quantitative detection of AFB1 and ZEN within 20 min by localizing two T lines on the NC membrane. Additionally, the implementation of Au-IgG indicative probe lessens the amount of the SERS nanotags, thereby saving manufacturing costs of SERS nanotags.

# 2. Experimental

Details of chemicals, reagents and instruments employed in the study are provided in the supplementary Material (S2.1., S2.2.). The experimental protocols including the preparation of Au-IgG (S2.3.), HPLC analysis of AFB1 and ZEN (S2.4.) are also included in Supplementary Material.

## 2.1 Synthesis of $Au^{MBA}$@Ag, $Fe_3O_4$ and magnetic SERS nanoprobes

### 2.1.1 Preparation of $Au^{MBA}$@Ag

AuNPs (~ 25 nm) were synthesized according to our previous work with slight alteration (Yin, et al., 2022). Firstly, solution of $HAuCl_4 \cdot 4H_2O$ (100 mL, 0.01%, w/v) was boiled then 1.6 mL of $Na_3C_6H_5O_7 \cdot 2H_2O$ (1%, w/v) was added quickly with continuous magnetic stirring. Once the color of mixture shifted to deep red, the AuNPs solution was further heated for extra 5 min and let to chill at room temperature (RT) for later procedure. Secondly, $Au^{MBA}$@Ag nanoparticles then prepared as follows (Yin, et al., 2023): 4-MBA ($10^{-4}$ M; 200 µL) was further gradually incorporated to AuNPs (20 mL) in addition to agitated for extra 40 min at RT. Subsequently, the prepared of $Au^{MBA}$NPs was spun-down using centrifuge at 7800 g for 15 min following resuspend with DDI water (20 mL). For Ag shell growth on the $Au^{MBA}$NPs, 400 µL of $Na_3C_6H_5O_7 \cdot 2H_2O$ (1%, m/v) and 1 mL of AA (10 mM) were supplemented to $Au^{MBA}$NPs solution (20 mL) at one time with vigorous stirring. Next, 1 mL of silver nitrate at 10 mM was implemented via a drop per 30 s to the combination at steady moving using stirrer (350 rpm) following by extra stirring for 20 min after fully adding $AgNO_3$. Finally, the precipitate of $Au^{MBA}$@Ag was moved out from the solution by

centrifugation at 7200 g for 20 min and resuspend with DDI water (20 mL)for further usage.

### 2.1.2 Preparation of $Fe_3O_4$ NPs

$Fe_3O_4$ magnetic nanoparticles ($Fe_3O_4$MNPs) were engineered via a adjusted solvothermal system according to the previous literature with few modification (Feng, et al., 2020). To summarize, 40 mL of ethylene glycol (EG) was mixed with $FeCl_3 \cdot 6H_2O$ (1.35 g) and magnetically agitated for 20 min until the mix was entirely dissolved. Subsequently, anhydrous sodium acetate (3.6 g) and PEG 400 (1g) were included and stirred for another 20 min until the whole constituents fully mixed. Afterward, the solution was sealed in Teflon-lined stainless steel autoclave (100 mL) and incubated at 210 ℃ for 6 hours. Once autoclave was chilled to RT, the product of black precipitate was picked upby a magnet and cleaned with ultrapure water as well as ethanol three periods, respectively. At last, the obtained precipitate was dehydrated at 60 ℃ for 4 hours in a vacuum oven.

### 2.3.3 Preparation of $Fe_3O_4$@PEI/$Au^{MBA}$@Ag

Refer to a previous literature (Tu, et al., 2023), a large number of $Au^{MBA}$@Ag may adhere to the external layer of $Fe_3O_4$ NPs via the intermediate layer of PEI. Here, 10 mg of fabricated $Fe_3O_4$MNPs was dispersed in the solution of PEI based in water (50 mL; 0.2 mg/mL) and ultrasonicated over 20 min to form positively charged $Fe_3O_4$@PEI. Once deionized water was used for purification twice, the magnetically product of $Fe_3O_4$@PEI was soaked in 10 mL ultrapure water ($Fe_3O_4$=1 mg/mL). Then, 200 μL of prepared $Fe_3O_4$@PEI was added to different volumes (1, 2, 3, 4 mL) of

183 $Au^{MBA}$@Ag colloidal solution containing 0.5% Tween-20 to obtain the optimal
184 adsorption capacity followed by the combining fluid was heavily vibrated using
185 ultrasonic for 20 min. Ultimately, the mixture was magnetically separated and
186 subsequently, 1 mL of ultrapure water containing 0.5% Tween-20 ($Fe_3O_4$=0.2 mg /mL)
187 was used to redisperse the precipitate. The obtained $Fe_3O_4$@PEI/$Au^{MBA}$@Ag were
188 stowed at 4 °C for more experiment.

189 **2.2 Preparation of magnetic SERS nanoprobes**

190 The second layer 4-MBA was labeled on the exterior of the aforementioned
191 magnetic particles ($Fe_3O_4$@PEI/$Au^{MBA}$@Ag) to introduce carboxyl group (-COOH)
192 which can be coupled with mAbs through the reaction of EDC/NHS reaction. In brief,
193 40 μL of 4-MBA ($10^{-4}$ M) was added dropwise to 1mL of $Fe_3O_4$@PEI/$Au^{MBA}$@Ag and
194 react for 1 h at RT. Later magnetic separation, the precipitate
195 ($Fe_3O_4$@PEI/$Au^{MBA}$@Ag-MBA) was redispersed in a buffer fluid of MES (1 mL,
196 pH=6.0 and 0.05 M). Then, 100 μL of activating solution encompassing (EDC and
197 NHS provided 0.1 mg/mL for each) was added and incubate the entire solution via
198 shaker at 37 ℃ for 30 min. Consequently, 8 μg of each AFB1-mAb and ZEN-mAb
199 were introduced to the $Fe_3O_4$@PEI/$Au^{MBA}$@Ag-MBA solution and continuously
200 shaken for 1 h at 37 °C. Next, 100 μL of solution containing BSA (1%, w/v) was
201 incorporated to block the excess -COOH sites for extra 30 min at 37 °C. Lastly, the
202 magnetic SERS nanoprobes ($Fe_3O_4$@PEI/$Au^{MBA}$@Ag-MBA-mAbs) were rinsed with
203 PBST (0.05%) under an external magnetic field and resuspended in PBS (400 μL, pH
204 7.4, 10 mM) holding 2% BSA (w/v), 5% trehalose, 2% PVP and 0.1 % Proclin 300.

The prepared SERS nanoprobes were kept at 4 °C for subsequent procedure.

**2.3 Assembly of LFIA strips**

The LFIA strip consisted of polyvinyl chloride (PVC) base plate, NC membrane, sample pad and absorbent pad (Fig. 1B(c)). It worth noting that, two test lines (T1 and T2) and a control line (C) were fabricated by spraying 0.2 mg/mL of each AFB1-BSA and ZEN-BSA in addition to goat anti-rabbit IgG (0.5 mg/mL) on NC membrane, which was firstly dissolved in PBS buffer (10 mM, pH 7.4). The application volume was adjusted at 1 μL/cm. Lately, the NC membrane adheres to the PVC base plates were dehydrated for 24 h at 37 °C. For construction LFIA strips, the sample pad and the absorbent pad were stuck on the PVC base plate joining an overlap of approximately 2 mm covering the NC membrane. Lastly, assembled card was snipped into 3.5 mm-wide LFIA strips and stockpiled in a vacuum sealed bag with a desiccant at 4 °C for future invstigations.

**2.4 SERS-LFIA detection system**

Herein, Fig. 1B clearly explain the phases for instantaneous detection of two mycotoxins (ZEN and AFB1) by means of diverse magnetic SERS nanoprobes. In this context, 500 μL of sample solution (or standard solution) was mixed with 10 μL each of the two magnetic SERS probes (AFB1 and ZEN SERS probes) in a 1.5 mL EP tube and the mix then incubated at RT with a period of 10 min. Next, the immunocomplex ($Fe_3O_4$@PEI/$Au^{MBA}$@Ag-MBA-mAb/target analyte) was enriched for 2 min by an exterior magnetic field and then resuspended with 100 μL of running buffer (0.01 M PBS, containing 1% BSA as well as 3% Tween-20). Furthermore, the suspension (100

μL) was relocated with in the micro-well. Next, 5 μL of prefabricated Au-IgG was added and mixed thoroughly. Then, the strip was submerged into the well. After 8 min, the sample pad was eradicated to finalize the immunochromatographic assay. Raman bands of T1 and T2 were acquired via a spectrometer of handheld Raman furnished by laser of 785 nm. Notably, the laser power was fixed at 50 mW and the integration time was 5 s. The Raman peak`s concentrations at 1074 $cm^{-1}$ (the characteristic band of 4-MBA) were attained from ten different spots over the test line and the average value was used for the quantitative analysis. Moreover, AccuRam® software was utilized to pre-handled every spectrum at baseline with flattening adjustment in order to eradicate apparatus noises. To calculate the standard deviation (SD) and average value, each trial was computed after three repetitions

**2.5 Assessment of SERS-LFIA strips for actual samples**

The practical applications of the SERS-LFIA strips for corn samples were evaluated by recovery experiment and comparative experiment. In the recovery experiment, the corn sample without AFB1 and ZEN determined by HPLC was used as the blank sample. Blank samples of corn flour (5g) were spiked with varying amount of mycotoxins (AFB1 and ZEN) solution to acquire equivalent spiked samples having AFB1 (1, 2.5, 5 μg/kg) and ZEN (30, 60, 120 μg/kg). The tainted samples was then stockpiled at RT for 2 h. Next, every tainted sample supplemented with 20 mL of 50% ethanol extraction and then vortexed for 5 min. After centrifuging at 1600 g for 5 min, the outcome supernatant was further diluted 5 times with PBST (0.01 M, pH 7.4, 0.1% Tween-20) for additionally detection. In the comparative

experiment, SERS-LFIA strips and the HPLC method were used to detect several positive corn actual samples adulterated with AFB1 and ZEN, and the results of the two methods were compared. The pre-treatment procedure of positive corn actual samples for SERS-LFIA detection was identical to that used for the spiked samples.

# 3. Results and Discussion

## 3.1 Principle of magnetic SERS-based LFIA strips

The preparation and testing principle of the proposed bi-channel magnetic SERS-LFIA system is illustrated in Fig. 1A novel magnetic SERS nanotag ($Fe_3O_4$@PEI/$Au^{MBA}$@Ag-MBA) was schemed and engineered through electrostatic adsorption of the PEI middle layer. This nanotag consisted of three parts: ~170 nm $Fe_3O_4$ core to generate a strong magnetic response, PEI interlayer to provide positive charge and improve the hydrophilicity of $Fe_3O_4$, a dual metallic core-shell structure embedded by 4-MBA ($Au^{MBA}$@Ag) to afford potent Raman signal. To further improve the Raman signal intensity and provide antibody binding sites, the second layer of 4-MBA was labeled on the surface of $Fe_3O_4$@PEI/$Au^{MBA}$@Ag to form the magnetic SERS nanotags. Two monoclonal antibodies (AFB1-mAb and ZEN-mAb) were coupled with the terminal carboxyl groups of 4-MBA on the SERS tags ($Fe_3O_4$@PEI/$Au^{MBA}$@Ag-MBA) directly via EDC/NHS reaction to form two magnetic SERS nanoprobes ($Fe_3O_4$@PEI/$Au^{MBA}$@Ag-MBA-mAb) (Fig. 1A). In addition, two coating antigens (AFB1-BSA and ZEN-BSA) as well as goat anti-rabbit IgG were correspondingly sprayed onto the NC membrane to form two T lines and a C line.

The quantitative detection of the two mycotoxins was achieved through the following three steps (Fig. 1B). First, two magnetic SERS nanoprobes were added to the sample solution (0.5 mL) and then endorsed to integrated with the target analytes during incubation. The resultant $Fe_3O_4$@PEI/$Au^{MBA}$@Ag-MBA-mAb/targets immunocomplex were enriched by the external magnetic field and resuspended in the running buffer. Second, the suspension had been transferred into the micro-well and copiously mixed with 5 μL of prefabricated Au-IgG. The immunochromatographic detection process started as the strip was inserted. If the sample solution did not contain target analytes, both magnetic SERS nanoprobes were captured by the corresponding coating antigen on the T lines, resulting in two dark black bands (T1 and T2). Conversely, if the sample solution contained target analytes, the two magnetic SERS nanoprobes first combined with the targets to form immunocomplexes, resulting in fewer magnetic SERS probes that could combine with the coating antigen on the T line and show light black bands. The added indicative probe Au-IgG can be captured by the secondary antibody on the C line and show a stable red, regardless of the amount of the target analytes. Ultimately, the SERS signals of the two T lines were evaluated using a handheld Raman spectrometer. Furthermore, antigen-antibody complex containing $Fe_3O_4$@PEI/$Au^{MBA}$@Ag-MBA SERS tags on the T lines can generate characteristic Raman peaks at 1074 $cm^{-1}$ when excited at 785 nm. Therefore, the sensitive quantitative detection of two mycotoxins can be succeeded by gaging Raman intensities of the characteristic peak on the two T lines.

### 3.2 Preparation and characterization of $Fe_3O_4$@PEI/$Au^{MBA}$@Ag-MBA

293 Core-shell structure embedded with 4-MBA ($Au^{MBA}$@Ag) and $Fe_3O_4$NPs were
294 well-structured, and then the assembly ($Fe_3O_4$@PEI/$Au^{MBA}$@Ag-MBA) was formed
295 through the PEI layer. A previous study reported that the Raman enhancement effect of
296 Au@Ag was prejudiced by the thickness of Ag (shell) as well as Au core dimension
297 (Peña-Rodríguez & Pal, 2011). Considerably, it was noted that the external layer of
298 metal NPs at thickness of (10~15 nm) attains the ideal Raman enhancement effect.
299 Herein, $Au^{MBA}$@Ag with the ideal Raman enhancement was synthesized according to
300 our previous research (Yin, et al., 2022). Evidently from Fig. 2A, the TEM image of
301 $Au^{MBA}$@Ag displayed a core-shell structure with a approximately 9 nm Ag shell as
302 well as monodispersed spherical structure. Besides, the statistical results of particle size
303 distribution (Fig. S1A) showed that the diameter of $Au^{MBA}$@Ag was 37.72±3.58 nm
304 and the RSD (n=30) was 9.49%, indicating that the synthesized nanoparticles have a
305 relatively uniform particle size. The 4-MBA as the Raman reporter molecules were
306 embedded in the bimetallic core-shell structures via Au-S covalent bonds to generate
307 strong Raman signals (Ma, et al., 2022). The EDS element mapping (Fig. 2B-C)
308 confirmed that Au, Ag and S elements coexist in $Au^{MBA}$@Ag, indicating the successful
309 preparation of $Au^{MBA}$@Ag. Previous studies have revealed that the UV-vis absorption
310 peaks of AuNPs and AgNPs were at ~ 520 nm and ~ 390 nm, respectively (Bhatt, Bhatt,
311 & Padmaja, 2018). The results showed that the absorption peak of AuNPs blueshifted
312 from 524 nm to 405 nm ($Au^{MBA}$@AgNPs) in the UV-vis spectra (Fig. S1B), indicating
313 the well-formation of core-shell structure.

314 Typically, $Fe_3O_4$NPs large size serve as the core, can provide a strong magnetic

response. As reported in Fig. 2D, $Fe_3O_4$NPs had a worthy dispersion and spherical structure, and the diameter was 178.15±24.20 nm and the RSD (n=16) was 13.58%. PEI is a cationic organic polymer rich in primary amine groups ($NH_2$), which can impart a strong positive charge to the electronegative $Fe_3O_4$NPs. In addition, PEI with good hydrophilicity also can greatly escalate the dispersibility of $Fe_3O_4$@PEI in aqueous solution (Wang, et al., 2019). Evidently from Fig. 2E, the diameter of $Fe_3O_4$@PEI/$Au^{MBA}$@Ag was 247.92±22.57 nm and the RSD (n=10) was 9.10%. As displayed in the magnified TEM image (Fig. 2F), numerous of electronegative $Au^{MBA}$@Ag were densely adsorbed onto the surface of $Fe_3O_4$@PEI. Additionally, high-angle annular dark-field scanning transmission electron microscopy (HADDF-STEM) clearly showed that many $Au^{MBA}$@Ag nanoparticles were distributed around the $Fe_3O_4$ core (Fig. 2G(i)). The EDS element mapping spectra further confirmed the elemental composition of $Fe_3O_4$@PEI/$Au^{MBA}$@Ag (Fig. 2G(ii-iv)), revealing that the magnetic core, composed of Fe (red) was densely surrounded by a significant amount of Au (blue) and Ag (yellow). In addition, the zeta potentials of $Fe_3O_4$, $Fe_3O_4$@PEI, $Au^{MBA}$@Ag and $Fe_3O_4$@PEI/$Au^{MBA}$@Ag were observed as -11.43 mV, 39.67 mV, -34.73 mV and -4.45 mV respectively, signifying that nanocomposites surface potential increased with PEI coating while decreased with adsorption of $Au^{MBA}$@Ag (Fig. 2H). These systematic fluctuations in the electrical features confirmed that the assembly between the $Fe_3O_4$ (core) and $Au^{MBA}$@Ag (satellites) was driven by the electrostatic interaction of the interlayer PEI.

The SERS activities of nanoparticles at each step were investigated with the

Raman intensities of the SERS nanotags since it is crucial for the detection of sensitivity and stability. Herein, 4-MBA with a large Raman cross section was selected as the Raman reporter molecule. Fig. 2I presents the typical Raman spectra of 4-MBA, the bands of bending and breathing vibration of aromatic rings appear at 1584 $cm^{-1}$ and 1074 $cm^{-1}$, respectively (Krajczewski, Michalowska, & Kudelski, 2020). As shown in Fig. 2I, $Au^{MBA}$@Ag could provide sufficiently strong Raman signals (curve b) while $Fe_3O_4$@PEI had no Raman signal (curve a), so the $Fe_3O_4$@PEI/$Au^{MBA}$@Ag assembled after adsorbing a large amount of $Au^{MBA}$@Ag that could generate stronger Raman signal (curve c). To facilitate the modification of antibodies, 4-MBA ($2^{nd}$ layer) with terminal carboxyl groups was labeled on the surface of $Fe_3O_4$@PEI/$Au^{MBA}$@Ag via stable Ag-S bonds. The outcomes indicated that the SERS probes (curve d-e) with modified antibodies had strong Raman signals owing to the loading of dual-layer Raman reporter molecules.

The absorbability of $Fe_3O_4$@PEI to $Au^{MBA}$@Ag directly affected the Raman intensities of SERS nanotags. Therefore, the maximum adsorbing capacity of $Fe_3O_4$@PEI was investigated by incubating different volumes (1 ~ 4 mL) of $Au^{MBA}$@Ag with the invariable amount of $Fe_3O_4$@PEI (1 mg/mL, 200 μL). According to the photographs in the adsorption process (Fig. S2A), it is evident that when the volume of $Au^{MBA}$@Ag was 3 mL and 4 mL, the remaining solution after magnetic separation was light yellow and dark yellow, indicating that excess $Au^{MBA}$@Ag were not adsorbed. In addition, the Raman intensities (characteristic peaks at 1074 $cm^{-1}$ and 1584 $cm^{-1}$) of the resuspension of the precipitate after magnetic separation were

consistent when the volume of $Au^{MBA}$@Ag was 3 mL and 4 mL (Fig. S2B-C). Therefore, the maximum adsorbing capacity of $Fe_3O_4$@PEI to $Au^{MBA}$@Ag was 3 mL. Moreover, the SERS enhancement factor (EF) of the $Fe_3O_4$@PEI/$Au^{MBA}$@Ag tags with maximum absorbability was calculated as $4.53 \times 10^7$ and the detailed calculation method is provided in the supporting information S3.3 (Table S2). Afterward, the magnetic response ability of $Fe_3O_4$@PEI/$Au^{MBA}$@Ag was investigated since it was crucial for the magnetic enrichment of analytes. As shown in Fig. S2D, the saturation magnetization of $Fe_3O_4$@PEI/$Au^{MBA}$@Ag was still as high as 33.15 emu/g to provide sufficient magnetic enrichment capacity. As the inserted picture displayed, the $Fe_3O_4$@PEI/$Au^{MBA}$@Ag nanoparticles were uniformly dispersed (a), enriched completely within 30 s by an external magnetic field (b), and returned to the dispersion state after removing the external magnetic field (c). Therefore, the superparamagnetic property and strong magnetic responsiveness of the $Fe_3O_4$@PEI/$Au^{MBA}$@Ag ensure rapid recovery of the magnetic immunocomplex from the sample solution in practical applications.

### 3.3 Construction and optimization of SERS-based LFIA strips

A micro-well lateral flow configuration was used in this investigation. Consequently, the LFIA test strip comprises only three portions: sample pad and absorbent pad as well as NC membrane; however, the conjugate pad is not included. Considering that the SERS nanotags ($Fe_3O_4$@PEI/$Au^{MBA}$@Ag-MBA) have a large diameter (247.92±22.57 nm), NC membrane with big pore sizes is necessary to ensure the effective transportation of the immunocomplex. ZEN SERS probes were used to

evaluate three common NC membrane (CN140, CN95 as well as 80 HP) with pore dimensions of 8 μm, 15 μm and 20 μm, in the lateral flow test. As presented in Fig. 3A, CN95 and 80 HP endorsed good transport of ZEN SERS probes, whereas some aggregates of ZEN SERS probes were visible at the intersection of the sample pad with CN140 membrane. However, the T line on the HP80 membrane was wider due to the larger pore sizes. In addition, Raman intensities on the T lines showed that the strongest signal was on the CN95 membrane, which was due to the loss of part of the SERS probes on the CN140 membrane and a slightly lower concentration of SERS probes on the 80HP membrane. Therefore, the CN95 membrane was chosen to construct LFIA strips. In addition, it was verified that the three probes can be specifically recognized by their respective antigens on the T lines. As shown in Fig. 3B(a), the two SERS probes were collected with the corresponding antigen on the T lines to form a clear black line, while the indicative probe Au-IgG was captured by the secondary antibody on the C line to form a red line, indicating that the three probes can be specifically recognized by their respective antigens. As shown in Fig. 3B(b), strong Raman signals (characteristic Raman spectra of 4-MBA) were detected on two T lines (curve ② and ③), further indicating specific binding between the antigens and corresponding SERS probes. However, no Raman signal was detected on the blank area and the C line (curve ① and ④), indicating good fluidity of the SERS probe on the CN95 membrane and the indicative probe only provided color but did not yield any Raman signal.

Thereafter, we further investigated the feasibility of simultaneous quantitative

403 detection of two mycotoxins using the bi-channel SERS-LFIA strip. Four standard
404 solutions of different concentrations were tested. The photographs of the test strips
405 (Fig. 3A(a)) revealed that the color of the two T lines changed with the concentration
406 of the target analytes. The test results were as follows: both AFB1 and ZEN at
407 concentration of 0 ng/mL, two dark T lines appeared (i), AFB1 at concentration of 1
408 ng/mL and ZEN at concentration of 20 ng/mL, the color of the corresponding T line
409 became lighter (ii-iii), AFB1 at concentration of 1 ng/mL and ZEN at concentration
410 of 20 ng/mL, respectively, the color of both T lines simultaneously lightened (iv).
411 The corresponding Raman spectra of the two T lines were verified and reported in
412 Fig. 3A(b). And the Raman intensities on T1 and T2 were adversely correlated with
413 the concentration of target analytes. These results substantiated that it was feasible to
414 quantitatively detect two mycotoxins simultaneously by monitoring the SERS
415 intensities on T1 and T2 lines.

416 Several key factors were then optimized including the concentration of the
417 coating antigens on T lines, the amount of antibodies modified on the SERS nanotags
418 and the volume of sample solution ($V_s$), to improve the detection performance of the
419 proposed SERS-LFIA strips. First, the concentration of the coating antigens was
420 optimized, since the concentration of antigen significantly affected the Raman
421 intensities on the T lines. Evidently from Fig. 4A, AFB1-BSA at ongoing
422 concentrations (0.1 to 0.3 mg /mL), T line progressively shifted darker and the
423 intensity of Raman peaks gradually augmented. Although at concentration ≥ 0.2 mg
424 /mL, Raman intensity tended to flat, too-high concentration caused the lower edge of

the T line to be darker. Therefore, the optimal concentration of AFB1-BSA was 0.2 mg/mL. Likewise, the optimal concentration of ZEN-BSA was also 0.2 mg/mL (Fig. 4B). Second, the amount of antibody modified on the SERS nanotags can influence the sensitivity of the competitive reaction and also the Raman intensity. Herein, the Raman intensities on the T line at AFB1 concentration of 0 ng/mL ($R_0$) and 1 ng/mL ($R_1$) and their ratios $R_0/R_1$ were collected to regulate the optimal amount of antibodies modified on the SERS nanotags. As revealed in Fig. 4C, the growth of $R_0$ tended to be stable at AFB1-antibody of 8 μg /mL and the value of $R_0/R_1$ was the maximum, indicating the highest sensitivity of the competitive reaction. Hence, the optimal amount of AFB1-antibody was 8 μg /mL. Likewise, the optimal concentration of ZEN-antibody was also 8 μg /mL (Fig. 4D). Third, the volume of the sample solution during incubation affected the concentration of the immunocomplex after magnetic separation and thus pretentious the sensitivity. Theoretically, too much volume of sample solution should be used to enrich the immunocomplex. However, it was discovered that an extensively large volume of the sample solution have adverse effects on magnetic enrichment, leading to extended magnetic collection times and greater loss of immunocomplex (Li, et al., 2022). As displayed in Fig. 4E(a), 10 μL each of the two magnetic SERS probes were added to 3 diverse amounts (0.5, 1.0 and 1.5 mL) of dilution buffer (10% ethanol). In the pre-treatment process of corn samples, the extraction solution was 50% ethanol. To maintain the activity of antibodies on the SERS nanoprobes, the extracted solution was diluted 5 times (10% ethanol) before being detected. Therefore, 10% ethanol was chosen as the dilution buffer to maintain a

consistent ethanol concentration. The three mixed solutions were incubated for 10 min. Thereafter, the magnetic SERS probes were collected at the bottom of the EP tube. Afterward, 100 μL of running buffer was added to resuspend the magnetic enrichment. In addition, an equal amount of SERS probes was directly added to 100 μL of running buffer as a comparison to inspect the influence of the sample solution volume on the loss of the magnetic enrichment. As the photographs of test strips shown in Fig. 4 E(a), the color of the T line was very similar to that of the comparison ($V_s$= 0.1 mL) while the $V_s$ was equal to 0.5 mL, but the color of the T lines was deteriorated while the Vs were equal to 1.0 mL and 1.5 mL. In addition, the intensities of Raman peaks on T lines were measured to further assess the resulting loss of the Raman signal. Compared with the comparison ($V_s$= 0.1 mL), the loss of Raman intensities on T lines was less than 5% while the $V_s$ was equal to 0.5 mL (Fig. 4E(b)), which was acceptable. However, the loss of Raman intensities on T lines were 11-15% and 45% while the Vs were equal to 1.0 mL and 1.5 mL (Fig. 4E(b)), respectively. Therefore, the optimal volume of sample solution during incubation is 0.5 mL. As such, the sensitivity which resulted on the immunocomplex was enriched five times as the sample solution can be concentrated from 0.5 mLto 0.1 mL by magnetic separation after incubation.

### 3.4 Detection performance evaluation of SERS-based LFIA strips

The magnetic SERS-based LFIA strips were used for the simultaneous detection of AFB1 and ZEN at the previously mentioned perfect conditions to evaluate several important performances, including sensitivity, uniformity, repeatability and specificity. A series of blended solutions with diverse quantities of AFB1 (0 ~0.5 ng /mL) and

ZEN (0 ~20 ng /mL) were investigated using the SERS-based LFIA strips to confirm the sensitivity of the proposed method. As displayed in Fig. 5A, uniform black color appeared on the T1 and T2 lines and the color intensity gradually weakened once the amount of the specified analyte in the standard solution enlarged. To accurately evaluate uniformity of the T line, the test strip with the darkest T line color (standard solution of 0 ng/mL) was selected as the evaluation object and the Raman intensities at 1074 $cm^{-1}$ from 10 various spots on the lines of T were acquired. Relative standard deviation (RSD) data of the Raman intensities were 1.23% and 1.49%, signifying good homogeneousness of the two T lines (Fig. 5B). Moreover, the negative and positive mixed standard solutions were checked with five strips to appraise the repeatability. The colors of the two T lines on the five test strips were basically consistent and the RSD values of the Raman intensity were less than 2%, indicating decent repeatability between them (Fig. 5C-D). Subsequently, we randomly measured 10 spots on one T line of a series of strips as shown in Fig. 5A, and averaged to generate the corresponding Raman spectra (Fig. 5E and F). Plainly, Fig. 5G(a) and Fig. 3H(a), depicts that Raman intensities of the distinctive spectrum at 1074 $cm^{-1}$ show an inverse relation with the AFB1 and ZEN quantities.This behavior followed the belief of competitive immunoassay, where the greater the analyte concentration, the less SERS probes were able to bind to the capture probes, subsequently inferior in the intensity of Raman peaks (Yin, et al., 2022). The calibration curves for AFB1 and ZEN were plotted by employing the relationship between $R/R_0$ and the logarithm of analytes (AFB1 or ZEN) concentration, where R and $R_0$ represented the Raman intensities of

491 standard solution at diverse concentrations and blank solution (0 ng/mL), respectively.
492 Furthermore, linearity range of AFB1 and ZEN were verified at 0.005 ~ 0.5 ng/mL and
493 0.2 ~ 20 ng /mL, respectively; as well as linear correlation coefficient ($R^2$) were
494 determined as following: AFB1 ($R^2$ = 0.99971) while ZEN ($R^2$ = 0.99712) (Fig. 5G(b)
495 and Fig. 5H(b)). The limit of detection (LOD) of the SERS-LFIA strips was
496 well-recognized as the concentration of analyte resulting in a 10% decrease in Raman
497 intensity compared with 0 ng/mL and was determined to be 0.095 ng /mL and 4.76 pg
498 /mL for ZEN and AFB1, respectively. Detection ranges of AFB1 and ZEN in corn
499 samples were determined to be 0.1-10 μg/kg as well as 4-400 μg/kg, correspondingly;
500 with LODs values as follows: for AFB1 (0.095 μg/kg) and ZEN (1.896 μg/kg) due to
501 implementation of a 20-fold dilution during sample processing.

502 The specificity of suggested SERS-LFIA system was investigated by detecting
503 other interfering mycotoxins (100 ng/mL), including DON, OTA and FB1, which
504 existed commonly in corn. As shown in Fig. 5I, only the target mycotoxins (AFB1=0.1
505 ng/mL and ZEN=2 ng/mL) were recognized by specific SERS probes, yielding lighter
506 colour with significant debilitated Raman intensity on the T lines. Furthermore, we
507 discovered that in spite of the interfering mycotoxins (DON, OTA, FB1) grasped 100
508 ng/mL, the colour and signal of Raman on T lines were consistent with the blank
509 control (0.01M PBS). Subsequently, these outcomes demonstrated that the engineered
510 SERS-LFIA system was highly specific to AFB1 and ZEN.

511 **3.5 Application in real corn samples.**

512 The spiked recovery experiments and confirmatory studies compared with HPLC

513 were carried out to evaluate the reliability and practical application of the fabricated
514 SERS-LFIA method for the detection of AFB1 and ZEN in corn samples. Specific
515 steps for AFB1 and ZEN detection using the HPLC apparatus are well-described in
516 supplementary material. Liquid chromatogram and corresponding standard curves for
517 AFB1 and ZEN were depicted in Fig. S3A and Fig. S4A, respectively. And the
518 correlation coefficients ($R^2$) were 0.99946 for AFB1 and 0.99977 for ZEN. The blank
519 corn sample employed in the spiked experiment was initially confirmed to be without
520 AFB1 and ZEN using the HPLC method (Fig. S3B(a) and Fig. S4B(a)). Table 1
521 highlighted the recovery rates of SERS-LFIA strips for spiked AFB1 (1.25, 2.5, 5.0,
522 7.5 μg/kg) and ZEN (30, 60, 120, 240 μg/kg) at four different concentrations:
523 91.28%-109.52% and 94.71%-108.15%, respectively, with RSDs less than 10%.
524 These discoveries revealed that the enrichment of immunocomplex by magnetic
525 SERS probes effectively reduced the matrix interference and obtained superior
526 accuracy and precision.

527 In addition to the spiked recovery experiment, several corn samples contaminated
528 with two mycotoxins were also detected to further verify the practical application of our
529 proposed SERS method. Herein, five positive corn samples (AFB1:1~10 μg/kg,
530 ZEN:40~400 μg/kg) were detected using each of the SERS-LFIA strips and HPLC
531 method. The result shows that there was good agreement between the two
532 methodologies' results, with coincidence rates ranging from 91.76% to 108.53%, and
533 RSDs less than 10% (Table 1). Moreover, the AFB1 and ZEN liquid chromatograms
534 of five positive contaminated corn samples are shown in Fig. S3B(b-f) and Fig.

S4C(b-f), respectively. Consequently, AFB1 and ZEN can be detected simultaneously and with high sensitivity by the SERS-LFIA system, which was established by enriching the target with magnetic SERS probes and integrating two T lines onto a single strip. In addition, the use of a handheld Raman spectrometer can yield results expeditiously, rendering our proposed method suitable for the rapid and on-site mycotoxins detection of corn samples.

The proposed method in this study exhibited satisfactory sensitivity since the LODs of AFB1 and ZEN were 4.76 pg/mL and 0.0948 ng/mL, respectively. Compared to earlier researchs of various mycotoxins detection in corn using SERS technology (Table S3), the sensitivity of this study is only inferior to one of the studies (Zheng, et al., 2022). But it could fully meet the strictest tolerable limits of AFB1 and ZEN (AFB1:0.1μg/kg, ZEN:20 μg/kg) in corn samples. In addition, superior detection accuracy (91.76% ~ 108.53%), precision (RSD < 10%) and fast detection speed (20 minutes) were obtained for the detection of positive corn samples which was believed to be a promising detection method in the future.

# 4. Conclusion

The current study developed a bi-channel magnetic SERS-based LFIA strip for the simultaneous detection of AFB1 and ZEN using $Fe_3O_4$@PEI/$Au^{MBA}$@Ag-MBA as active SERS nanotags. The novel SERS nanotag, composed of a large-sized $Fe_3O_4$ core and double-layer Raman reporter molecules (4-MBA), demonstrated excellent stability, good dispersity, strong magnetic responsiveness and superior SERS activity. Two specific antibodies were modified on SERS nanotags to serve as both separation tools

and SERS sensing labels for quantitative analysis of AFB1 and ZEN. The magnetic enrichment function of SERS probes significantly increased the detection sensitivity and reduced the interference of the sample matrix, thereby achieving lower LODs of 4.76 pg/mL for AFB1 and 0.0948 ng/mL for ZEN. The detection ranges of AFB1 and ZEN in corn samples were determined to be 0.1-10 μg/kg and 4-400 μg/kg, with LODs of 0.095 μg/kg for AFB1 and 1.896 μg/kg for ZEN owing to the implementation of a 20-fold dilution during sample processing. The LODs were significantly lower than the most stringent MRLs of AFB1 (0.1 μg/kg) and ZEN (20 μg/kg) in baby grain food.

Additionally, the SERS-based LFIA system employed two probes: SERS probes loaded with Raman reporter molecules and indicative probes of rabbit IgG-modified gold nanoparticles. The two probes were utilized for quantitative detection of target analytes and availability assessment of test strips, respectively. The unique design of two probes effectively enhanced the utilization efficiency of SERS nanotags and reduced detection costs. Conclusively, the method demonstrated satisfactory recoveries in spiked experiments and exhibited good coincidence rates as compared to the HPLC method for contaminated corn samples detection. This method is thought to be a potent tool for on-site detection of AFB1 and ZEN in corn using portable Raman spectrometry owing to its high sensitivity, specificity, simplicity, and ability to simultaneously analyze two mycotoxins.

# Acknowledgments

The authors acknowledge the financial support provided by the National Natural Science Foundation of China (51975259), the Outstanding Young Teachers of Blue

579 Project in Jiangsu Province, the Postgraduate Research and Practice Innovation
580 Program of Jiangsu Province (KYCX21_3383).

581

# References


Bhatt, R., Bhatt, R., & Padmaja, P. (2018). DTPA capped gold and silver nanofluids-facile synthesis and their application as chromium sensors. *Sensors and Actuators B: Chemical, 258*, 602-611. https://doi.org/10.1016/j.snb.2017.11.154.

Chen, R., Du, X., Cui, Y., Zhang, X., Ge, Q., Dong, J., & Zhao, X. (2020). Vertical Flow Assay for Inflammatory Biomarkers Based on Nanofluidic Channel Array and SERS Nanotags. *Small, 16*(32), 2002801. https://doi.org/10.1002/smll.202002801.

Chen, X., Leng, Y., Hao, L., Duan, H., Yuan, J., Zhang, W., Huang, X., & Xiong, Y. (2020). Self-assembled colloidal gold superparticles to enhance the sensitivity of lateral flow immunoassays with sandwich format. *Theranostics, 10*(8), 3737-3748. https://doi.org/10.7150/thno.42364.

Feng, J., Xu, Y., Huang, W., Kong, H., Li, Y., Cheng, H., & Li, L. (2020). A magnetic SERS immunosensor for highly sensitive and selective detection of human carboxylesterase 1 in human serum samples. *Analytica Chimica Acta, 1097*, 176-185. https://doi.org/10.1016/j.aca.2019.11.004.

Guo, J., Chen, S., Guo, J., & Ma, X. (2021). Nanomaterial Labels in Lateral Flow Immunoassays for Point-of-Care-Testing. *Journal of Materials Science & Technology, 60*, 90-104. https://doi.org/10.1016/j.jmst.2020.06.003.

Guo, Z., Wu, X., Jayan, H., Yin, L., Xue, S., El-Seedi, H. R., & Zou, X. (2024). Recent developments and applications of surface enhanced Raman scattering spectroscopy in safety detection of fruits and vegetables. *Food Chemistry, 434*, 137469. https://doi.org/10.1016/j.foodchem.2023.137469.

Ji, C., Fan, Y., & Zhao, L. (2016). Review on biological degradation of mycotoxins. *Animal Nutrition, 2*(3), 127-133. https://doi.org/10.1016/j.aninu.2016.07.003.

Kebede, H., Liu, X., Jin, J., & Xing, F. (2020). Current status of major mycotoxins contamination in food and feed in Africa. *Food Control, 110, 106975*. https://doi.org/10.1016/j.foodcont.2019.106975.

Kim, K., Kashefi-Kheyrabadi, L., Joung, Y., Kim, K., Dang, H., Chavan, S. G., Lee, M.H., & Choo, J. (2021). Recent advances in sensitive surface-enhanced Raman scattering-based lateral flow assay platforms for point-of-care diagnostics of infectious diseases. *Sensors and Actuators B: Chemical, 329*. https://doi.org/10.1016/j.snb.2020.129214.

Ko, J., Lee, C., & Choo, J. (2015). Highly sensitive SERS-based immunoassay of aflatoxin B1 using silica-encapsulated hollow gold nanoparticles. *Journal of Hazardous Materials, 285*, 11-17. https://doi.org/10.1016/j.jhazmat.2014.11.018.

Krajczewski, J., Michalowska, A., & Kudelski, A. (2020). Star-shaped plasmonic nanostructures: New, simply synthetized materials for Raman analysis of surfaces. *Spectrochim Acta A Mol Biomol Spectrosc, 225*, 117469. https://doi.org/10.1016/j.saa.2019.117469.

Lee, S. H., Hwang, J., Kim, K., Jeon, J., Lee, S., Ko, J., Lee, J., Kang, M., Chung, D. R., & Choo, J. (2019). Quantitative Serodiagnosis of Scrub Typhus Using Surface-Enhanced Raman Scattering-Based Lateral Flow Assay Platforms. *Analytical Chemistry, 91*(19), 12275-12282. https://doi.org/10.1021/acs.analchem.9b02363.

Li, J., Wu, T., Wang, C., Tu, J., Song, X., Shao, Y., Wang, C., Qi, K., & Xiao, R. (2022). Nanogapped Fe3O4@Au Surface-Enhanced Raman Scattering Tags for the Multiplex Detection of Bacteria on an Immunochromatographic Strip. *ACS Applied Nano Materials, 5*(9), 12679-12689. https://doi.org/10.1021/acsanm.2c02494.

Liu, B., Ni, H., Zhang, D., Wang, D., Fu, D., Chen, H., Gu, Z., & Zhao, X. (2017). Ultrasensitive Detection of Protein with Wide Linear Dynamic Range Based on Core-Shell SERS Nanotags and Photonic Crystal Beads. *ACS Sensors, 2*(7), 1035-1043. https://doi.org/10.1021/acssensors.7b00310.

Liu, B., Zheng, S., Liu, Q., Gao, B., Zhao, X., & Sun, F. (2022). SERS-based lateral flow immunoassay strip for ultrasensitive and quantitative detection of acrosomal protein SP10. *Microchemical Journal, 175, 107191*. https://doi.org/10.1016/j.microc.2022.107191.

Liu, S., Dou, L., Yao, X., Zhang, W., Zhao, M., Yin, X., Sun, J., Zhang, D., & Wang, J. (2020). Nanozyme amplification mediated on-demand multiplex lateral flow immunoassay with dual-readout and broadened detection range. *Biosensors and Bioelectronics, 169, 112610*. https://doi.org/10.1016/j.bios.2020.112610.

Liu, X., Yang, X., Li, K., Liu, H., Xiao, R., Wang, W., Wang, C., & Wang, S. (2020). Fe3O4@Au SERS tags-based lateral flow assay for simultaneous detection of serum amyloid A and C-reactive

protein in unprocessed blood sample. *Sensors and Actuators B: Chemical, 320, 128350*. https://doi.org/10.1016/j.snb.2020.128350.

Ma, L., Han, E., Yin, L., Xu, Q., Zou, C., Bai, J., Wu, W., & Cai, J. (2023). Simultaneous detection of mixed pesticide residues based on portable Raman spectrometer and Au@Ag nanoparticles SERS substrate. *Food Control, 153, 109951*. https://doi.org/10.1016/j.foodcont.2023.109951.

Ma, W., Liu, L., Zhang, X., Liu, X., Xu, Y., Li, S., & Zeng, M. (2022). A microfluidic-based SERS biosensor with multifunctional nanosurface immobilized nanoparticles for sensitive detection of MicroRNA. *Analytica Chimica Acta, 1221, 340139*. https://doi.org/10.1016/j.aca.2022.340139.

Pazos, E., Garcia-Algar, M., Penas, C., Nazarenus, M., Torruella, A., Pazos-Perez, N., Guerrini, L., Vázquez, M. E., Garcia-Rico, E., Mascareñas, J. L., & Alvarez-Puebla, R. A. (2016). Surface-Enhanced Raman Scattering Surface Selection Rules for the Proteomic Liquid Biopsy in Real Samples: Efficient Detection of the Oncoprotein c-MYC. *Journal of the American Chemical Society, 138*(43), 14206-14209. https://doi.org/10.1021/jacs.6b08957.

Peña-Rodríguez, O., & Pal, U. (2011). Enhanced plasmonic behavior of bimetallic (Ag-Au) multilayered spheres. *Nanoscale Research Letters, 6*(1), 279. https://doi.org/10.1186/1556-276X-6-279.

Rebellato, A. P., dos Santos Carames, E. T., Lima Pallone, J. A., & Rocha, L. d. O. (2021). Mycotoxin bioaccessibility in baby food through in vitro digestion: an overview focusing on risk assessment. *Current Opinion in Food Science, 41*, 107-115. https://doi.org/10.1016/j.cofs.2021.03.010.

Ren, W., Mohammed, S. I., Wereley, S., & Irudayaraj, J. (2019). Magnetic Focus Lateral Flow Sensor for Detection of Cervical Cancer Biomarkers. *Analytical Chemistry, 91*(4), 2876-2884. https://doi.org/10.1021/acs.analchem.8b04848.

Su, L., Hu, H., Tian, Y., Jia, C., Wang, L., Zhang, H., Wang, J., & Zhang, D. (2021). Highly Sensitive Colorimetric/Surface-Enhanced Raman Spectroscopy Immunoassay Relying on a Metallic Core-Shell Au/Au Nanostar with Clenbuterol as a Target Analyte. *Analytical Chemistry, 93*(23), 8362-8369. https://doi.org/10.1021/acs.analchem.1c01487.

Tu, J., Wu, T., Yu, Q., Li, J., Zheng, S., Qi, K., Sun, G., Xiao, R., & Wang, C. (2023). Introduction of multilayered magnetic core-dual shell SERS tags into lateral flow immunoassay: A highly stable and sensitive method for the simultaneous detection of multiple veterinary drugs in complex samples. *Journal of Hazardous Materials, 448, 130912*. https://doi.org/10.1016/j.jhazmat.2023.130912.

Wang, C., Wang, C., Wang, X., Wang, K., Zhu, Y., Rong, Z., Wang, W., Xiao, R., & Wang, S. (2019). Magnetic SERS Strip for Sensitive and Simultaneous Detection of Respiratory Viruses. *ACS Applied Materials & Interfaces, 11*(21), 19495-19505. https://doi.org/10.1021/acsami.9b03920.

Wang, J., Guan, H., Han, Q., Tan, S., Liang, Q., & Ding, M. (2019). Fabrication of Yb3+-Immobilized Hydrophilic Phytic-Acid-Coated Magnetic Nanocomposites for the Selective Separation of Bovine Hemoglobin from Bovine Serum. *ACS Biomaterials Science & Engineering, 5*(6), 2740-2749. https://doi.org/10.1021/acsbiomaterials.9b00074.

Wang, J., Jiang, C., Jin, J., Huang, L., Yu, W., Su, B., & Hu, J. (2021). Ratiometric Fluorescent Lateral Flow Immunoassay for Point-of-Care Testing of Acute Myocardial Infarction. *Angewandte Chemie-International Edition, 60*(23), 13042-13049. https://doi.org/10.1002/anie.202103458.

Wang, L., Wang, X., Cheng, L., Ding, S., Wang, G., Choo, J., & Chen, L. (2021). SERS-based test strips: Principles, designs and applications. *Biosensors and Bioelectronics, 189*, 113360. https://doi.org/10.1016/j.bios.2021.113360.

Wang, X., Choi, N., Cheng, Z., Ko, J., Chen, L., & Choo, J. (2017). Simultaneous Detection of Dual Nucleic Acids Using a SERS-Based Lateral Flow Assay Biosensor. *Analytical Chemistry, 89*(2), 1163-1169. https://doi.org/10.1021/acs.analchem.6b03536.

Xie, H., Wang, X., van der Hooft, J. J. J., Medema, M. H., Chen, Z.-Y., Yue, X., Zhang, Q., & Li, P. (2022). Fungi population metabolomics and molecular network study reveal novel biomarkers for early detection of aflatoxigenic Aspergillus species. *Journal of Hazardous Materials, 424, 127173*. https://doi.org/10.1016/j.jhazmat.2021.127173.

Xing, C., Dong, X., Xu, T., Yuan, J., Yan, W., Sui, X., & Zhao, X. (2020). Analysis of multiple mycotoxins-contaminated wheat by a smart analysis platform. *Analytical Biochemistry, 610*, 113928. https://doi.org/10.1016/j.ab.2020.113928.

Xing, K.-Y., Shan, S., Liu, D.-F., & Lai, W.-H. (2020). Recent advances of lateral flow immunoassay for mycotoxins detection. *Trac Trends in Analytical Chemistry, 133, 116087*. https://doi.org/10.1016/j.trac.2020.116087.

Xu, J., Li, W., Liu, R., Yang, Y., Lin, Q., Xu, J., Shen, P., Zheng, Q., Zhang, Y., Han, Z., Li, J., & Zheng, T. (2016). Ultrasensitive low-background multiplex mycotoxin chemiluminescence

immunoassay by silica-hydrogel photonic crystal microsphere suspension arrays in cereal samples. *Sensors and Actuators B: Chemical, 232*, 577-584. https://doi.org/10.1016/j.snb.2016.03.123.

Yang, Y., Ren, M.-Y., Xu, X.G., Han, Y., Zhao, X., Li, C.-H., & Zhao, Z.-L. (2022). Recent advances in simultaneous detection strategies for multi-mycotoxins in foods. *Critical Reviews in Food Science and Nutrition*. https://doi.org/10.1080/10408398.2022.2137775.

Yin, L., You, T., Arslan, M., El-Seedi, H. R., Guo, Z., Zou, X., & Cai, J. (2023). Dual-layers Raman reporter-tagged Au@Ag combined with core-satellite assemblies for SERS detection of Zearalenone. *Food Chemistry, 429, 136834*. https://doi.org/10.1016/j.foodchem.2023.136834.

Yin, L., You, T., El-Seedi, H. R., El-Garawani, I. M., Guo, Z., Zou, X., & Cai, J. (2022). Rapid and sensitive detection of zearalenone in corn using SERS-based lateral flow immunosensor. *Food Chemistry, 396, 133707*. https://doi.org/10.1016/j.foodchem.2022.133707.

Zhang, D., Huang, L., Liu, B., Ge, Q., Dong, J., & Zhao, X. (2019). Rapid and Ultrasensitive Quantification of Multiplex Respiratory Tract Infection Pathogen via Lateral Flow Microarray based on SERS Nanotags. *Theranostics, 9*(17), 4849-4859. https://doi.org/10.7150/thno.35824.

Zhang, W., Tang, S., Jin, Y., Yang, C., He, L., Wang, J., & Chen, Y. (2020). Multiplex SERS-based lateral flow immunosensor for the detection of major mycotoxins in maize utilizing dual Raman labels and triple test lines. *Journal of Hazardous Materials, 393, 122348*. https://doi.org/10.1016/j.jhazmat.2020.122348.

Zhou, Q., & Tang, D. (2020). Recent advances in photoelectrochemical biosensors for analysis of mycotoxins in food. *Trac Trends in Analytical Chemistry, 124, 115814*. https://doi.org/10.1016/j.trac.2020.115814.

# Figure Captions

**Fig. 1.** Schematic illustration of the bi-channel magnetic SERS-LFIA system. (A) Schematic presentation of the preparation of two SERS probes. (B) The design of $Fe_3O_4$@PEI/$Au^{MBA}$@Ag-MBA-based SERS-LFIA strips for simultaneous detection of two mycotoxins.

**Fig. 2.** (A) TEM image of $Au^{MBA}$@Ag and the approximate thickness of the Ag shell. (B) The EDS element mapping images of Au, Ag and S. (C) Elemental analysis of the $Au^{MBA}$@Ag by EDS. (D) TEM image of $Fe_3O_4$. (E) TEM image and (F) magnified TEM image of $Fe_3O_4$@PEI/$Au^{MBA}$@Ag. (G) High-angle annular dark-field image of $Fe_3O_4$@PEI/$Au^{MBA}$@Ag (i) and EDS element mapping images of Fe (ii), Au (iii) and Ag (iv). (H) Zeta potential of the nanoparticles in the preparation. (I) SERS spectra of $Fe_3O_4$@PEI (a), $Au^{MBA}$@Ag (b), $Fe_3O_4$@PEI/$Au^{MBA}$@Ag (c) and antibodies-modified magnetic SERS probes (d-e).

**Fig. 3.** (A) Comparison of three NC membranes, photograph (a) and corresponding SERS intensities at 1074 $cm^{-1}$ on the T line (b). (B) Specificity evaluation between SERS probes and capture antigens, photographs (a) and SERS intensities on the blank zone, T1 line, T2 line and C line (b). (C) Feasibility investigation of the simultaneous detection of two mycotoxins, photograph (a) and corresponding SERS intensities at 1074 $cm^{-1}$ on T1 line and T2 line (b).

**Fig. 4.** (A) Optimization of the concentration of AFB1-BSA. (B) Optimization of the amount of AFB1-mAb. (C) Optimization of the concentration of ZEN-BSA. (D)

Optimization of the amount of ZEN-mAb. (E) Determination of the volume of sample solution during incubation, photographs of incubation process and test strips (a); and corresponding SERS intensities of different volume of sample solution at 1074 $cm^{-1}$ on T1 and T2 lines (b).

**Fig. 5.** (A) Photographs of test strips for the detection of various concentrations of AFB1 and ZEN. (B) Raman intensities of the characteristic peak of 4-MBA at 1074 $cm^{-1}$ from 10 different spots on the T lines. (C) Photograph of five test strips for negative mixed standard solution detection and corresponding Raman intensity on T lines. (D) Photograph of five test strips for positive mixed standard solution detection and corresponding Raman intensity on T lines. (E-F) Average Raman spectra on two T lines for different concentrations of AFB1 and ZEN detection. (G-H) Corresponding calibration curves of AFB1 and ZEN based on the relationship between $R/R_0$ at 1074 $cm^{-1}$ and the concentration of analytes. Error bars indicate the standard deviations measured from three separate experiments. (I) Evaluation of the anti-interference of SERS-based LFIA strips against other common mycotoxins.

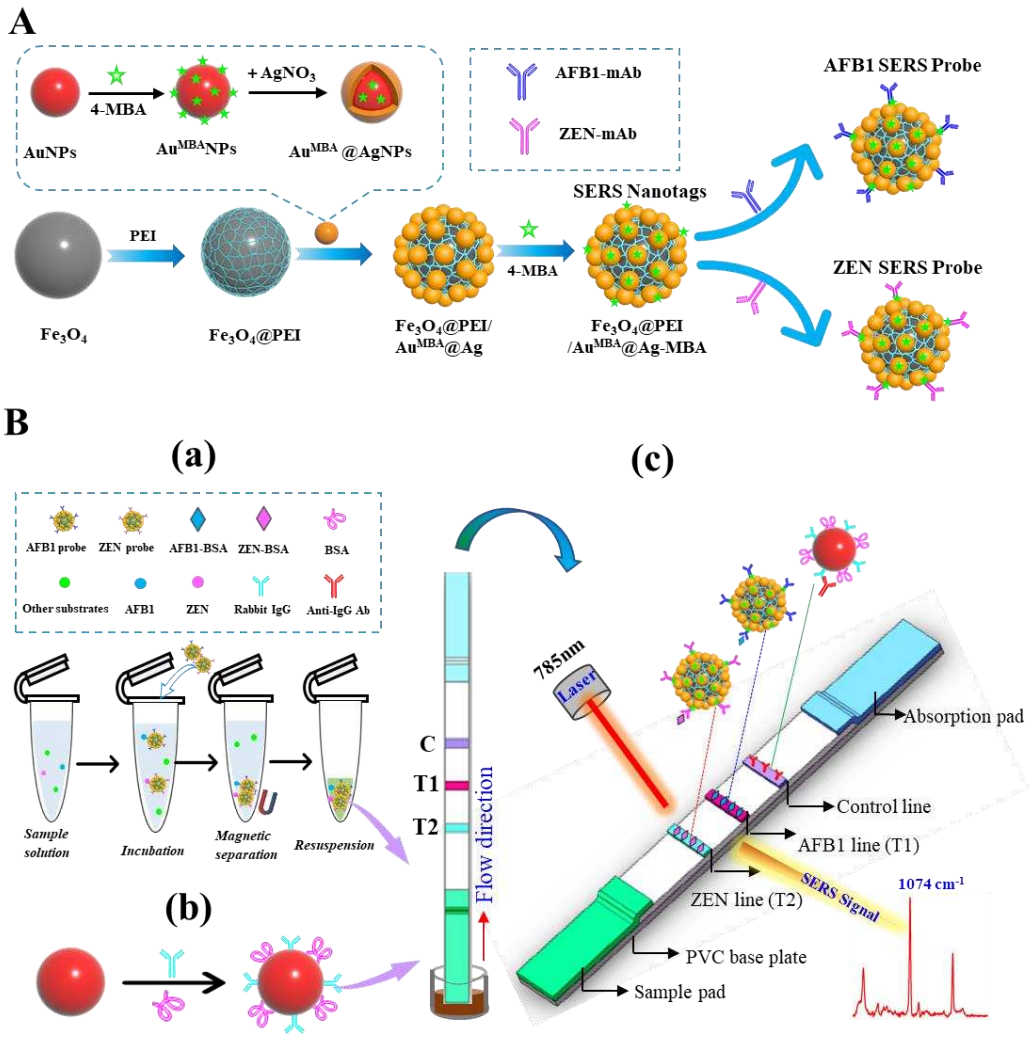


**Fig. 1.** Schematic illustration of the bi-channel magnetic SERS-LFIA system. (A) Schematic presentation of the preparation of two SERS probes. (B) The design of $Fe_3O_4$@PEI/$Au^{MBA}$@Ag-MBA-based SERS-LFIA strips for simultaneous detection of two mycotoxins.

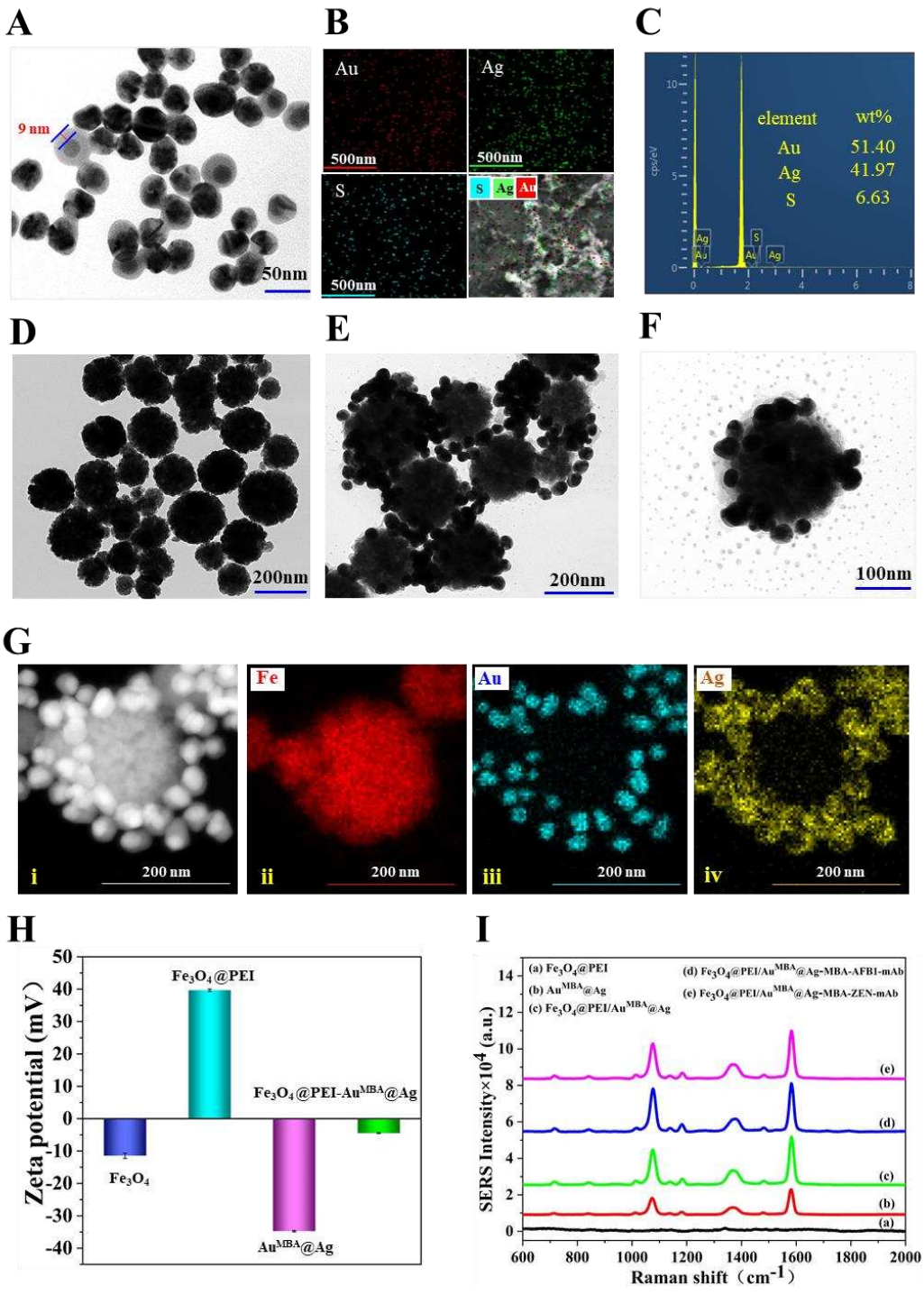


**Fig. 2.** (A) TEM image of $Au^{MBA}$@Ag and the approximate thickness of the Ag shell. (B) The EDS element mapping images of Au, Ag and S. (C) Elemental analysis of the $Au^{MBA}$@Ag by EDS. (D) TEM image of $Fe_3O_4$. (E) TEM image and (F) magnified TEM image of $Fe_3O_4$@PEI/$Au^{MBA}$@Ag. (G) High-angle annular dark-field image of

$Fe_3O_4$@PEI/$Au^{MBA}$@Ag (i) and EDS element mapping images of Fe (ii), Au (iii) and Ag (iv). (H) Zeta potential of the nanoparticles in the preparation. (I) SERS spectra of $Fe_3O_4$@PEI (a), $Au^{MBA}$@Ag (b), $Fe_3O_4$@PEI/$Au^{MBA}$@Ag (c) and antibodies-modified magnetic SERS probes (d-e).

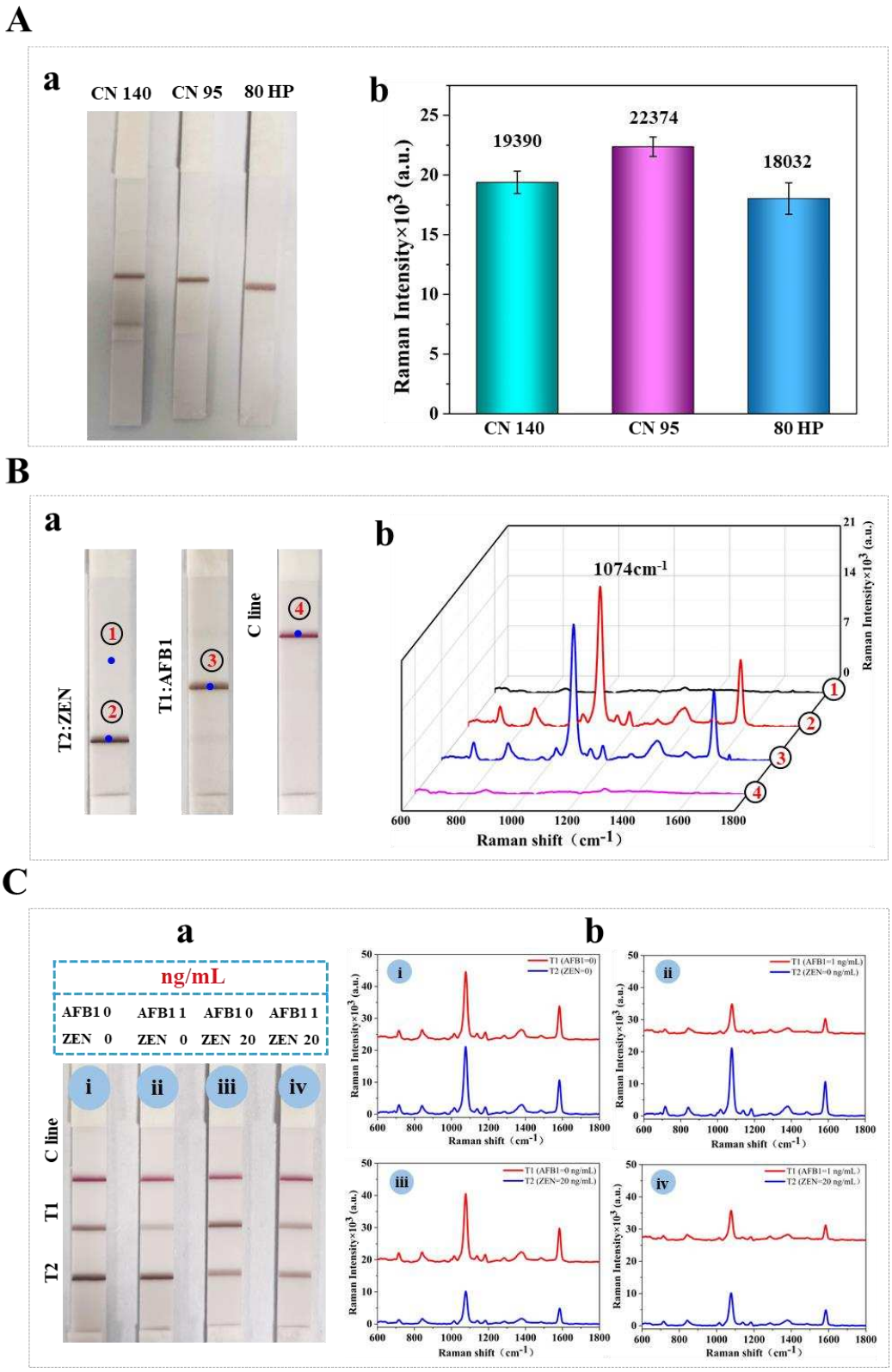


**Fig. 3.** (A) Comparison of three NC membranes, photograph (a) and corresponding SERS intensities at 1074 $cm^{-1}$ on the T line (b). (B) Specificity evaluation between

SERS probes and capture antigens, photographs (a) and SERS intensities on the blank zone, T1 line, T2 line and C line (b). (C) Feasibility investigation of the simultaneous detection of two mycotoxins, photograph (a) and corresponding SERS intensities at 1074 $cm^{-1}$ on T1 line and T2 line (b).

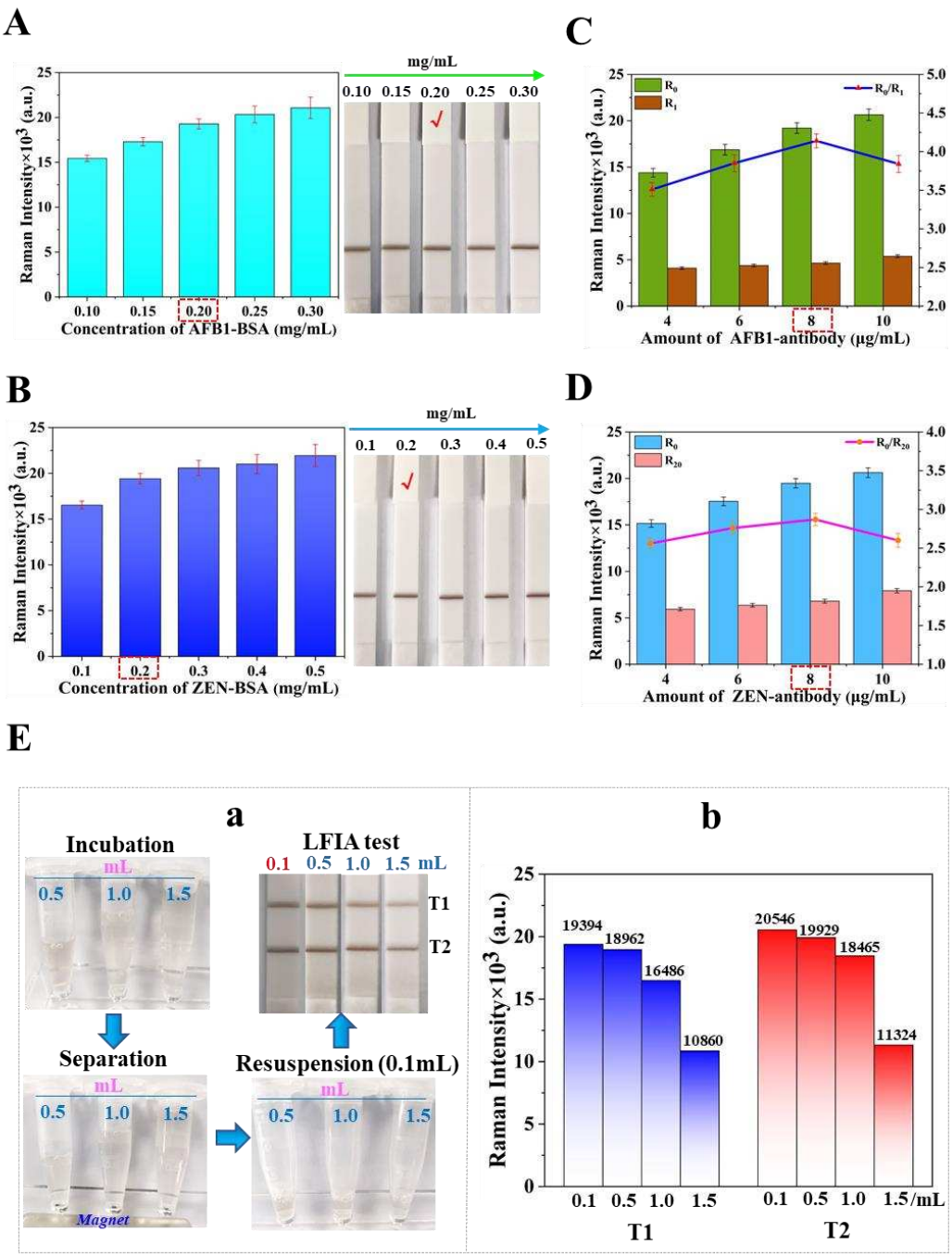


**Fig. 4.** (A) Optimization of the concentration of AFB1-BSA. (B) Optimization of the concentration of ZEN-BSA. (C) Optimization of the amount of AFB1-mAb. (D) Optimization of the amount of ZEN-mAb. (E) Determination of the volume of sample solution during incubation, photographs of incubation process and test strips (a); and

corresponding SERS intensities of different volume of sample solution at 1074 $cm^{-1}$ on T1 and T2 lines (b).

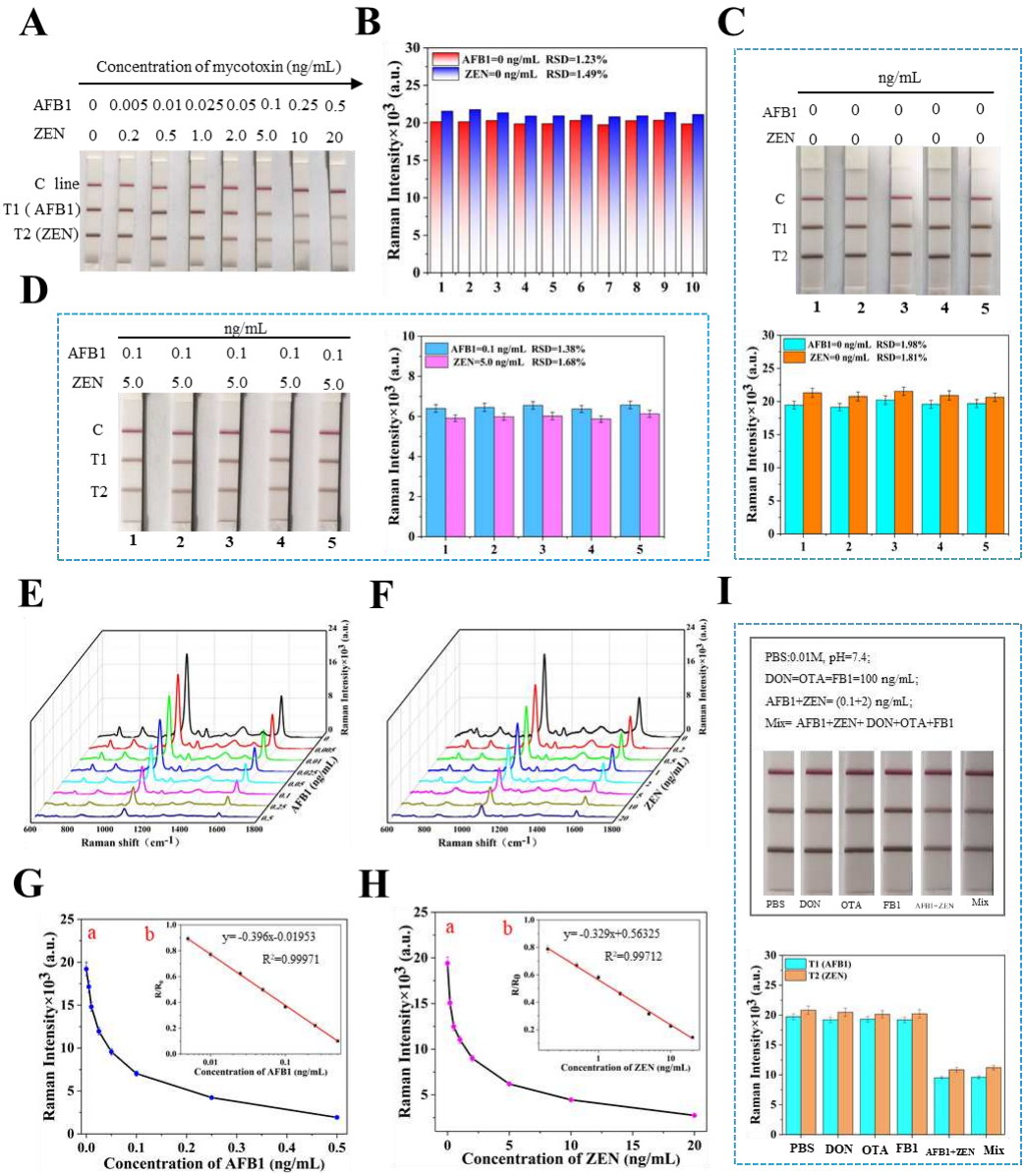


**Fig. 5.** (A) Photographs of test strips for the detection of various concentrations of AFB1 and ZEN. (B) Raman intensities of the characteristic peak of 4-MBA at 1074 $cm^{-1}$ from 10 different spots on the T lines. (C) Photograph of five test strips for negative mixed standard solution detection and corresponding Raman intensity on T lines. (D) Photograph of five test strips for positive mixed standard solution detection and corresponding Raman intensity on T lines. (E-F) Average Raman spectra on two T lines for different concentrations of AFB1 and ZEN detection. (G-H) Corresponding

calibration curves of AFB1 and ZEN based on the relationship between $R/R_0$ at 1074 $cm^{-1}$ and the concentration of analytes. Error bars indicate the standard deviations measured from three separate experiments. (I) Evaluation of the anti-interference of SERS-based LFIA strips against other common mycotoxins.

# Table Caption

**Table 1** The recoveries and verification results for the detection of two mycotoxins in spiked corn samples and contaminated corn samples with the SERS-LFIA strips (n=3) and HPLC method.

**Table 1** The recoveries and verification results for the detection of two mycotoxins in spiked corn samples and contaminated corn samples with the SERS-LFIA strips (n=3) and HPLC method.

| **Samples** | **Mycotoxins** | **Spiked (μg/kg)** | **SERS-LFIA strips** | | |
|---|---|---|---|---|---|
| | | | **Detected (μg/kg)** | **Recovery (%)** | **RSD (%)** |
| Spiked corn samples | AFB1 | 1.25 | 1.171 | 93.68 | 9.47 |
| | | 2.5 | 2.282 | 91.28 | 9.42 |
| | | 5.0 | 5.476 | 109.52 | 8.19 |
| | | 7.5 | 7.925 | 105.67 | 9.67 |
| | ZEN | 30 | 32.163 | 107.21 | 9.13 |
| | | 60 | 64.891 | 108.15 | 8.34 |
| | | 120 | 113.655 | 94.71 | 9.51 |
| | | 240 | 252.734 | 105.31 | 9.25 |
| **Samples** | **Mycotoxins** | **HPLC** | **SERS-LFIA strips** | | |
| | | **Detected (μg/kg)** | **Detected (μg/kg)** | **Recovery (%)** | **RSD (%)** |
| Contaminated corn samples | 1#-AFB1 | 1.802 | 1.901 | 105.49 | 8.12 |
| | 1#-ZEN | 46.985 | 50.296 | 107.05 | 7.96 |
| | 2#-AFB1 | 3.395 | 3.161 | 93.11 | 7.37 |
| | 2#-ZEN | 355.536 | 371.762 | 104.56 | 6.59 |

| | | | | |
|---|---|---|---|---|
| 3#-AFB1 | 4.620 | 5.014 | 108.53 | 7.64 |
| 3#-ZEN | 199.597 | 183.146 | 91.76 | 8.52 |
| 4#-AFB1 | 5.462 | 5.236 | 95.86 | 8.29 |
| 4#-ZEN | 256.602 | 236.751 | 92.26 | 9.17 |
| 5#-AFB1 | 8.173 | 8.547 | 104.58 | 7.43 |
| 5#-ZEN | 160.562 | 150.758 | 93.89 | 9.14 |